Decreasing CO2 partial pressure triggered Mg–Fe–Ca carbonate formation in ancient Martian crust preserved in the ALH84001 Meteorite

Article · February 2011

DOI: 10.1111/j.1468-8123.2010.00296.x

CITATIONS
11

READS
117

4 authors, including:

Jan-Michael Ilger
Museum für Naturkunde Dortmund
15 PUBLICATIONS **138** CITATIONS
SEE PROFILE

Yunjiao Fu
Technische Universität Clausthal
19 PUBLICATIONS **306** CITATIONS
SEE PROFILE

Carsten Hansen
Consulaqua Hamburg
29 PUBLICATIONS **482** CITATIONS
SEE PROFILE

GEOFLUIDS

Geofluids (2010) doi: 10.1111/j.1468-8123.2010.00296.x

Decreasing CO_2 partial pressure triggered Mg–Fe–Ca carbonate formation in ancient Martian crust preserved in the ALH84001 Meteorite

W. VAN BERK[1], J.-M. ILGER[1], Y. FU[1] AND C. HANSEN[2]

[1]*Department of Geology and Paleontology, Clausthal University of Technology, Clausthal-Zellerfeld, Germany;* [2]*Department of Water Resources Management, Rhenish-Westfalian Institute for Water, Mülheim an der Ruhr, Germany*

ABSTRACT

We retrace hydrogeochemical processes leading to the formation of Mg–Fe–Ca carbonate concretions (first distinct carbonate population, FDCP) in Martian meteorite ALH84001 by generic hydrogeochemical equilibrium and mass transfer modeling. Our simple conceptual models assume isochemical equilibration of orthopyroxenite minerals with pure water at varying water-to-rock ratios, temperatures and CO_2 partial pressures. Modeled scenarios include CO_2 partial pressures ranging from 10.1325 to 0.0001 MPa at water-to-rock ratios between 4380 and 43.8 mol mol^{-1} and different temperatures (278, 303 and 348 K) and enable the precipitation of Mg–Fe–Ca solid solution carbonate. Modeled range and trend of carbonate compositional variation from magnesio-siderite (core) to magnesite (rim), and the precipitation of amorphous SiO_2 and magnetite coupled to magnesite-rich carbonate are similar to measured compositional variation. The results of this study suggest that the early Martian subsurface had been exposed to a dynamic gas pressure regime with decreasing CO_2 partial pressure at low temperatures (approximately 1.0133 to 0.0001 MPa at 278 K or 6 to 0.0001 MPa at 303 K). Moderate water-to-rock ratios of ca. 438 mol mol^{-1} and isochemical weathering of orthopyroxenite are additional key prerequisites for the formation of secondary phase assemblages similar to ALH84001's 'FDCP'. Outbursts of water and $CO_{2(g)}$ from confined ground water in fractured orthopyroxenite rocks below an unstable CO_2 hydrate-containing cryosphere provide adequate environments on the early Martian surface.

Key words: ALH84001, carbonates, carbon dioxide, groundwater, Martian crust, modeling

Received 7 December 2009; accepted 21 April 2010

Corresponding author: Wolfgang van Berk, Department of Geology and Paleontology, Clausthal University of Technology, Leibnizstraße 10, D-38678 Clausthal-Zellerfeld, Germany.
Email: wolfgang.van-berk@tu-clausthal.de. Tel: +49 5323 72 2234. Fax: +49 5323 72 2903.

Geofluids (2010)

INTRODUCTION AND AIM

Martian meteorite ALH84001 is the only sample of ancient Martian crust available for scientific analyses. Altered orthopyroxenite displays clear evidence for intense water–rock–CO_2 interactions resulting in the formation of secondary carbonates. These Mg–Fe–Ca carbonates (thin section 311; ALH84001.119) are present at approximately 1 vol% exhibiting four textural types, including concretions displaying a distinct and widely ranging compositional zoning with magnetite and pyrite inclusions (specified as 'first distinct carbonate population', FDCP; Eiler *et al.* 2002). FDCP constitutes approximately 0.2–0.5 vol% of ALH84001 and is concentrated on the surfaces of fractures found throughout a heavily shocked orthopyroxenite (Eiler *et al.* 2002) consisting of orthopyroxene, olivine, maskelynite, chromite, pyrite and apatite (Harvey & McSween 1994; Mittlefehldt 1994; McKay *et al.* 1996; Table 1). Crystallization age of orthopyroxenite in ALH84001 is estimated to be 4.5 Gyr (Nyquist *et al.* 2001) and FDCP formation 0.5–0.6 Gyr later (Corrigan & Harvey 2004). The first ALH84001 shock event is speculated to be 4.0 Gyr in age (Ash *et al.* 1996), and is argued to have caused a fracture surface in the orthopyroxenite (McKay *et al.* 1996). Major element analyses of FDCP (Fig. 1) indicate the distinct range and compositional zoning trend of FDCP. Magnesio-siderite cores of FDCP concretions, approximately 20–200 μm in diameter, are surrounded by a black band which is 5–10 μm thick and rich in magnetite inclusions. This black band is surrounded by a white band,

Table 1 Modeling reactor's mineral phase assemblage.

		Composition	
		(mol)	(mol%)
$MgSiO_3$	Enstatite	0.0927*	
$FeSiO_3$	Ferrosilite	0.0271	
$CaSiO_3$	Wollastonite	0.0037*	
$En_{0.75}Fs_{0.22}Wo_{0.03}$		0.1235	97.0
Mg_2SiO_4	Forsterite	0.0006	
Fe_2SiO_4	Fayalite	0.0002	
$Fo_{0.75}Fa_{0.25}$		0.0008	0.6
$NaAlSi_3O_8$	Albite	0.0002	
$CaAl_2Si_2O_8$	Anorthite	0.0001	
Maskelynite		0.0003	0.2
FeS_2	Pyrite	0.0006	0.5
$Ca_5(PO_4)_3OH$	Hydroxyapatite	0.0015	1.2†
(Fe, Mg)Cr_2O_4 chromite		0.0006	0.5‡
		0.1273	100.0

*Including enstatite and wollastonite components in lesser quantities of Augite ($En_{45}Wo_{43}$; Meyer 2003).
†Assumed preferential dissolution of apatite. Measured apatite content is approximately 0.2 wt% (Meyer 2003).
‡Chromite is assumed to be nonreactive under modeling conditions and is excluded from equilibrium calculations. A total of 0.1267 mol in modeling reactor's mineral phase assemblage leads to a water-to-rock ratio of 438 mol mol^{-1}.

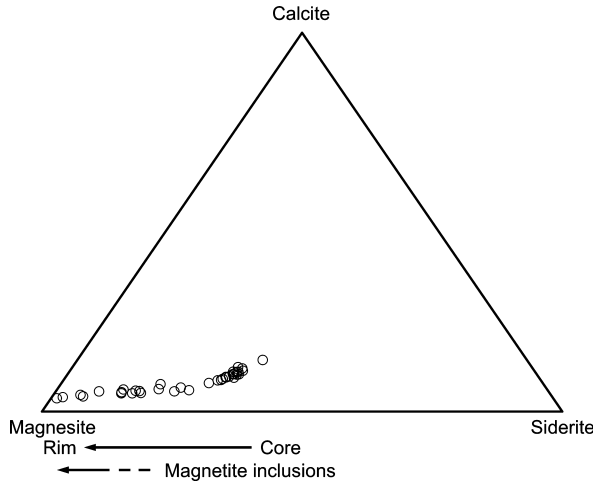

Fig. 1. Major element composition of ALH84001 carbonates ('first distinct carbonate population'). Data (Eiler *et al.* 2002) are rearranged; MnCO3 component (0.2–8.0 mol%) is omitted and ternary composition is normalized to 100 mol%. Compositional range displaying magnetite inclusions is marked.

10–15 μm thick and composed of Mg-rich carbonate. Finally, a second black, inclusion-rich band typically forms the concretion rims (Eiler *et al.* 2002). Amorphous silica is homogeneously distributed throughout the ALH84001 carbonate (Westall *et al.* 1998; Greenwood & McSween 2001; Bernas *et al.* 2005). 'Smectite-type clay' is detectable near some carbonate globules (Thomas-Keprta *et al.* 1997), and secondary pyrite is associated with secondary carbonate (Greenwood *et al.* 2000).

The conditions under which the carbonate's observed compositional zoning formed are still debated. Numerous formation hypotheses for the origin of carbonate in ALH84001 have been proposed including: (i) high-temperature processes such as shock melting of pre-existing carbonates (Scott *et al.* 1998; Scott 1999), (ii) metamorphic conversion of mafic silicates at temperatures >923 K (Harvey & McSween 1996), (iii) biogenic origin at low temperatures (McKay *et al.* 1996), (iv) precipitation from aqueous fluids at low temperatures (273–573 K; Mittlefehldt 1994; Romanek *et al.* 1994; Treiman 1995; Valley *et al.* 1997; Treiman & Romanek 1998), and (v) precipitation near 273 K due to evaporation (McSween & Harvey 1998; Warren 1998).

Experimental work has shown that chemically zoned carbonate globules and iron sulfides are produced at 423 K from multiple fluxes of aqueous Ca–Mg–Fe–CO_2–S solutions displaying different compositions (Golden *et al.* 2001). Magnetite crystals were formed by subsequent decomposition of previously precipitated Fe-rich carbonates by brief heating to 743 K (Golden *et al.* 2001). Experiments at 298 K produced poorly crystalline Fe carbonates and globules of Mg calcite during 24 or 96 h of reaction time in response to varying starting compositions of CO_2-saturated aqueous solutions containing Mg^{2+}, Fe^{2+} and Ca^{2+}ions (Golden *et al.* 1999). These experimental results indicate that CO_2-saturated aqueous solutions containing varying concentrations Mg^{2+}, Fe^{2+} and Ca^{2+}might provide hydrogeochemical conditions enabling the precipitation of chemically zoned Mg–Fe–Ca carbonate from aqueous solutions.

Molar ratios of Mg to Ca and Fe to Ca in aqueous solutions interacting with a rock with similar composition to the ALH84001 meteorite have been modeled (Niles *et al.* 2006). Modeling results indicate that Fe-, Mg-rich aqueous solutions interacting with ultramafic rock at high carbon dioxide partial pressures (pCO_2) must have a lower pH (<7) and a low temperature (<373 K) to eventually precipitate Mg–Fe–Ca carbonate similar to ALH84001's FDCP carbonates. Niles *et al.* (2006) proposed an upwelling of subsurface CO_2-rich solutions which could have induced subsurface aqueous alteration of ALH8400-type rock.

The aim of this work was to identify hydrogeochemical processes enabling activities of dissolved $species_{(aq)}$ to achieve ion activity products greater than Mg–Fe–Ca carbonate's solubility products. Modeled composition of phase assemblages (including solid solution carbonate) results from modeled activities of dissolved $species_{(aq)}$. We will identify prerequisites for the formation and preservation of phase assemblages similar to ALH84001's secondary minerals in a water–orthopyroxenite system which is exposed to varying pCO_2, water-to-rock ratios and temperatures. Our modeling aims not to retrace the exact mecha-

nisms of Mg–Fe–Ca carbonate formation (i.e. equilibrium versus nonequilibrium). Rather, by comparing modeled composition of phase assemblages – resulting from modeled activities of dissolved species$_{(aq)}$ – with FDCP's phase assemblage, possible conditions of FDCP's formation in ancient Martian crust are identified. FDCP's distinct compositional zoning trend and coexisting secondary phase assemblage, including magnetite and amorphous silica, are the key signals to be retraced by hydrogeochemical reaction path modeling based on chemical thermodynamics.

Simple isochemical initial conditions are prerequisites for our modeling. Our generic modeling scenarios do not focus on a set of predefined physical and chemical conditions (e.g. temperature and pCO_2) proposed by previous formation hypotheses. We intend instead to identify and quantify pCO_2, temperature and water-to-rock ratios leading to the formation of ternary solid solution carbonate and an associated secondary phase assemblage similar to ALH84001's FDCP.

MODELING CONCEPT AND APPROACH

Our modeling concept includes an open batch reactor which is filled by a phase assemblage of primary mineral phases (total amount of 0.1267 mol excluding chromite content; according to the orthopyroxenite composition and its porosity; Table 1) and 1.0 kg of pure water (55.51 mol H_2O; pH 7.0) leading to a water-to-rock ratio of 438 mol mol^{-1}. Rock alteration is limited to the fringes of ALH84001's fissures where minor amounts of rock forming minerals are exposed to the aqueous solution filling the cracks. Therefore, we consider high conceptual water-to-rock ratios.

Hydroxyapatite is relatively enriched in the phase assemblage of the reactor as it is a sensitive phase for dissolution in comparison with olivine and pyroxene (Hurowitz & McLennan 2007) and maskelynite or plagioclase (Dreibus *et al.* 1996). Leaching experiments (at 293 and 394 K; pH 7 under $N_{2(g)}$ and pH 4 under $CO_{2(g)}$ atmospheres) indicated that phosphorus is highly extractable from original meteorite material unaffected by previous aqueous leaching (Mautner & Sinaj 2002). The reactor's coexisting primary mineral phase assemblage and pure water are exposed to CO_2 partial pressures which are decreasing from 10.1325 to 0.0001 MPa, increasing from 0.0001 to 10.1325 MPa, or constant at 0.1013 MPa. Isothermal conditions (278, 303 and 348 K) or decreasing temperature (348 to 278 K; coupled to constant or decreasing pCO_2; Table 2) characterize the temperature regime. Complete and suppressed re-equilibration between the aqueous solution and mineral phases is considered in different scenarios.

In summary, modeling constraints reflect an isochemical and low-temperature water–rock interaction in a dynamic CO_2 pressure regime. The modeling approach assumes 'local thermodynamic equilibrium' of the primary mineral phase assemblage with secondary minerals (complete re-equilibration), $CO_{2(g)}$ and the evolving composition of the aqueous solution. Conceptually, the equilibration and coupled mass transfer are driven by the reaction with (and system's loss or gain of) $CO_{2(g)}$ in response to a stepwise decrease or increase in pCO_2. Secondary mineral phases can precipitate from the aqueous solution at saturation. Ternary solid solution carbonate (components: calcite, magnesite and siderite), amorphous silica ($SiO_{2(a)}$), magnetite and Ca montmorillonite (a 'smectite-type clay') are chosen as potential secondary mineral phases. Rhodochrosite is not considered as a component of solid solution carbonate, as no Mn^{2+}-bearing primary mineral phase has been quantified in ALH84001 meteorite. Pyrophyllite, talc, vivianite, kaolinite, diaspore, leonhardite, sepiolite and other SiO_2 phases, which have not been identified in ALH84001 meteorite, are excluded from calculation of equilibrium species distribution and mass

Table 2 Modeling scenarios.

	PWoE*		pCO_2 (MPa log pCO_2)		Water-to-rock ratio (mol mol^{-1})			
Scenario	CRE†	SRE‡	Decrease	Increase	4380	438	43.8	t (K)
r-d-438-303	×		1.0 to −4.0			×		303
r-d-4380-303	×		1.0 to −4.0		×			303
r-d-43.8-303	×		1.0 to −4.0				×	303
r-d-438-278	×		1.0 to −4.0			×		278
r-d-438-348	×		1.0 to −4.0			×		348
r-i-438-303	×			−4.0 to 1.0		×		303
s-d-438-303		×	1.0 to −4.0			×		303
r-d-438-348/278	×		1.0 to −4.0			×		348 to 278
r-c-438-348/278	×		Constant at −1			×		348 to 278

Scenario names indicate: (i) re-equilibration or suppressed re-equilibration ('r-' or 's-'), (ii) decreasing, increasing or constant CO_2 partial pressure ('d-' or 'i-' or 'c-'), (iii) water-to-rock ratio ('4380-', '438-' or '43.8-') and (iv) temperature or temperature range ('303', '278', '348' or '348-278').
*Pathway of equilibration with mineral phases.
†Complete re-equilibration.
‡Suppressed re-equilibration.

transfer. Although dolomite, aragonite, calcite, magnesite and siderite are lacking as secondary mineral phases in our model, the hydrogeochemical modeling considers these pure mineral phases. Calculated saturation indices ($SI = \log(IAP(K_S^g)^{-1}$); see Tables S1–S9; modeling input files) clearly indicate that dolomite, aragonite, calcite, magnesite and siderite never achieve saturation as pure phases at modeled conditions ($SI < 0$). Thus, integration of these carbonate phases into the model's list of secondary mineral phases would not effect modeled equilibrium species distribution and mass transfer.

We have modeled several different scenarios for various temperatures, pCO_2, and water-to-rock ratios (Table 2). The control of the aqueous solution composition and resulting composition of the mineral phase assemblage are based solely on chemical thermodynamics. Although we investigated several models (not discussed in this paper) with different compositions of the starting solution, we found that the effects of solution composition on the precipitated type and amount of secondary minerals were negligible. Therefore, we use pure water in each scenario.

Under a dynamic pCO_2 regime, two different equilibria with mineral phases can be modeled. One assumes re-equilibration of secondary and remaining primary mineral phases in response to changing pCO_2 and corresponding aqueous composition. For example, a precipitated solid solution carbonate phase, with its distinct composition, can be completely dissolved when pCO_2 and the aqueous composition have changed. In parallel, a new equilibrium solid solution carbonate phase with a modified composition is formed. Therefore, complete re-equilibration with compositional zoning of solid solution carbonate phases is prevented as long as phase dissolution and growth are not kinetically controlled (see discussion in Corrigan & Harvey 2004). Kinetic aspects are excluded from our modeling approach, and some implications of this exclusion are discussed below. The second pathway of equilibration with mineral phases excludes re-equilibration of precipitated solid solution carbonate. Thereby, newly formed solid solution carbonate phase compositions remain in dis-equilibrium with the altered composition of the aqueous solution and the pCO_2 conditions. Changing hydrogeochemical conditions thus causes compositional zoning of modeled solid solution carbonate phases. The two modeling scenarios emphasize how different reaction pathways control the compositional variation of carbonate concretions.

The PHREEQC computer code (Parkhurst & Appelo 1999) is applied to calculate equilibrium species distribution among aqueous solutions, solids and gas phases based on chemical thermodynamics for aqueous solutions. Equilibrium species distribution and coupled mass transfer to achieve equilibrium, as a function of specified reversible and irreversible geochemical reactions, are calculated by applying homogenous and heterogeneous mass-action equations, and related temperature-dependent equilibrium constants. Equilibrium constants are derived from basic thermodynamic data. The program uses a modified Newton–Raphson method to solve the nonlinear equation system including mass-action equations, mol-balance equations and charge balances. Calculated mass transfer and resulting equilibrium species distribution are achieved if: (i) the activities of all $species_{(aq)}$ involved fulfill mass-action equations according to their equilibrium constants, (ii) the molalities of all $species_{(aq)}$ and phases fulfill mol- or mass-balances for all elements involved, and (iii) the molalities of all ionic $species_{(aq)}^{+/-}$ fulfill charge-balance equation. Equilibrium species distribution is characterized in terms of molalities and activities of aqueous species, pH, pe, ion activity products and the type and amount of solid and gaseous phases dissolved or precipitated. The code supports activity coefficients calculated according to an extended form of the Debye–Hückel equation that is reliable for aqueous solutions with an ionic strength less than 0.7 mol kgw^{-1}. Temperature effects on equilibrium constants are calculated using PHREEQC's option 'analytical expressions' (for details, see Parkhurst & Appelo 1999). Control of total pressure (not pCO_2) over solubility equilibria of solid phases and on equilibria of aqueous species distribution is not considered by PHREEQC ($p_{total} = 0.1013$ MPa); possible effects resulting from this simplification are discussed in the following text.

Equilibrium reactions and corresponding equilibrium constants, along with their temperature dependences for all aqueous species, solids and gas phases are listed in the thermodynamic database 'wateq4f.dat' (Parkhurst & Appelo 1999). Equilibrium constants for enstatite, forsterite and fayalite, which are not included in the 'wateq4f.dat' database, are recalculated considering published data (for details, see Supplementary Table S1). Data for wollastonite are taken from the database 'minteq.dat' (Parkhurst & Appelo 1999).

Calculations of composition and mass transfer of solid solution carbonate at equilibrium assume ideal behavior of all components (or end-members: calcite, magnesite and siderite). The activity of each end-member solid is equal to its mole fraction, and miscibility gaps are not considered. The composition of solid solution carbonate results from calculated equilibrium species distribution. As noted above, two different pathways of equilibration with mineral phases are considered. The first assumes complete re-equilibration among solids, pCO_2, and altered aqueous solutions. In the second, (newly) precipitated solid solution carbonate phase is excluded from the altered aqueous solution and pCO_2. Therefore, re-equilibration is prevented when calculating a new equilibrium species distribution driven by a decreased pCO_2. The pathway of equilibration with mineral phases, pCO_2, water-to-rock ratio, and temperature are variables in the modeling scenarios (Table 2). These scenarios and

Table 3 Excerpt from PHREEQC input file Table S1 for modeling scenario r-d-438-303 including detailed explanatory notes (bold).

TITLE r-d-438-303
PHASES
 # Equilibrium constants for enstatite, forsterite, and fayalite, which are not included in the 'wateq4f.dat' database; recalculated considering published data. Data for wollastonite are taken from the database 'minteq.dat' (Parkhurst & Appelo 1999).
Enstatite
G°f = −1459.0 kJ mol^{-1}
data from http://www.osti.gov/energycitations/product.biblio.jsp?osti_id=5274849
$MgSiO_3 + 2H^+ + H_2O = Mg^{+2} + H_4SiO_4$
log_*k* 13.19
Fayalite
G°f = −1379.4 kJ mol^{-1}
data from Stumm, W. & Morgan, J. J. Aquatic Chemistry, John Wiley, New York, 2nd edn., 1981.
$Fe_2SiO_4 + 4H^+ = 2Fe^{+2} + H_4SiO_4$
log_*k* 16.647
Ferrosilite
G°f = −1117.82 kJ mol^{-1}
data from Boyd T. D. & Scott S. D. Microbial and hydrothermal aspects of ferric oxyhydroxides # and ferrosic hydroxides: the example of Franklin # Se-amount, Western Woodlark Basin, Papua New
Guinea. *Geochem. Trans.* **7** (2001). DOI: 10.1039/bm.
$FeSiO_3 + 2H^+ + H_2O = Fe^{+2} + H_4SiO_4$
log_*k* 7.11
Wollastonite
log_*k* = 12.996
from Minteq.dat
Parkhurst, D. L. & Appelo, C. A. J. User's guide to PHREEQC (Version 2) – A computer program
for speciation, batch reaction, one-dimensional transport, and inverse geochemical
calculations. *U.S. Geological Survey Water-Resources Investigations Report* **99-4259** (1999).
$CaSiO_3 + 2H^+ + H_2O = Ca^{+2} + H_4SiO_4$
log_*k* 12.996
delta_h −19.498 kcal
SELECTED_OUTPUT
-file r-d-438-303.XLS
-equilibrium_phases Enstatite Ferrosilite Wollastonite Forsterite Fayalite Albite
Anorthite Pyrite Hydroxyapatite $CO_{2(g)}$ Magnetite $SiO_{2(a)}$
Montmorillonite-Ca
-saturation_indices Dolomite
-solid_solutions calcite magnesite siderite
#----------first modeling step (pCO_2 = 100 atm)
SOLUTION 1
 # Starting solution; pure water
-pH 7.0
-density 1.000
-temp 30.0
-units mmol kgw^{-1}
EQUILIBRIUM_PHASES 1
 # Primary phases(s; g) involved in equilibrium calculation at starting conditions

Enstatite	0.0	0.0927
Ferrosilite	0.0	0.0271
Wollastonite	0.0	0.0037
Forsterite	0.0	0.0006
Fayalite	0.0	0.0002
Albite	0.0	0.0002
Anorthite	0.0	0.0001
Pyrite	0.0	0.0006
Hydroxyapatite	0.0	0.0015

 # log pCO_2 (equivalent to 100 atm)
$CO_{2(g)}$ 2.00
 # Secondary phases(s) involved in equilibrium calculation at starting conditions
 # Phase assemblage is free of secondary phases at starting conditions

Table 3 (Continued).

#	Saturation Index		# Amount in phase # assemblage [mol]
Magnetite	0.0	0.0	
$SiO_{2(a)}$	0.0	0.0	
Montmorillonite-Ca	0.0	0.0	

SOLID_SOLUTIONS 1
 # Secondary phase involved in equilibrium calculation at starting conditions
 # Phase assemblage is free of TernarySolidSolution carbonate at starting conditions

TernarySolidSolution	
-comp Calcite	0.0
-comp Magnesite	0.0
-comp Siderite	0.0

SAVE solution 2
SAVE solid_solutions 2
END
#---------- first modeling step (pCO_2 = 100 atm)
#---------- second modeling step (pCO_2 = 80 atm)
USE solution 2
USE SOLID_SOLUTIONS 2
#changed composition of orthopyroxenite
 # Primary phases(s; g) involved in equilibrium calculation after the first modeling step
 # Composition of altered orthopyroxenite
EQUILIBRIUM_PHASES 2

#	Saturation Index	Amount in phase assemblage [mol]
Enstatite	0.0	0.0
Ferrosilite	0.0	0.0
Wollastonite	0.0	0.0
Forsterite	0.0	0.0
Fayalite	0.0	0.0
Anorthite	0.0	0.0
Hydroxyapatite	0.0	0.0
Pyrite	0.0	5.999E−04
Magnetite	0.0	0.0
$SiO_{2(a)}$	0.0	1.226E−01
Montmorillonite-Ca	0.0	1.714E−04

 # log pCO_2 (equivalent to 80 atm)
$CO_{2(g)}$ 1.90
 # Unchanged temperature
REACTION_TEMPERATURE
30
SAVE solution 3
SAVE SOLID_SOLUTIONS 3
END
#---------- second modeling step (pCO_2 = 80 atm)

hydrogeochemical models are presented in PHREEQC input files attached (Tables S1–S9) which present a complete and detailed description and documentation of PHREEQC calculations. Utilizing PHREEQC's key words 'SAVE solution', 'SAVE solid solution', 'USE solution' and 'USE solid solution' enable the user to model re-equilibration of the solid solution carbonate and coexisting aqueous solution along decreasing pCO_2 (for details, see Tables 3 and S1). Modeling of suppressed re-equilibration with secondary carbonate is achieved using PHREEQC's key words 'SAVE solution' and 'USE solution' (for details, see Table S7). Table 3 presents a short excerpt from the PHREEQC input file in Table S1 and includes detailed explanatory notes.

Due to insufficient modeling capabilities our calculations ignore the effect of total pressure (differing from 0.1013 MPa) on equilibrium constants. The effect of varying total pressure on equilibrium constants can be assessed by differences regarding the solubility of calcite. Renard *et al.* (2005) calculated that the equilibrium constant of calcite increases by a factor of 1.26 for an increase in system total pressure from 0.1013 to 10.1325 MPa in pure water at 298 K. Owen & Brinkley (1941) included the partial molar volumes of dissolved species ($Ca^{2+}_{(aq)}$ and $CO^{2-}_{3(aq)}$) in their calculation of calcite solubility at high pressures. The resulting equilibrium constant of calcite increases by a factor of 2.8 for an increase in system pressure from 0.1013 to ~50 MPa in an aqueous NaCl solution at 298 K. Thus, the effects of total pressure on equilibration can be neglected.

The assumption of thermodynamic equilibrium and ideal behavior of components in solid solution carbonate is also questionable. Moreover, heterogeneous solid solutions can persist in metastable equilibrium with the aqueous solution. No kinetic aspects are considered in our modeling. Reaction time is a key factor which controls the precipitation of FDCP concretions in the ALH84001 meteorite. FDCP's compositional zoning might reflect dynamic and short-term processes of precipitation, dissolution or complete and incomplete re-equilibration. Experiments at room temperature (298 K) produced poorly crystalline Fe carbonates and globules of Mg calcite during 24 or 96 h of reaction time in response to varying starting compositions of CO_2-saturated aqueous solutions containing Mg^{2+}, Fe^{2+} and Ca^{2+}ions (Golden *et al.* 1999). Romanek *et al.* (2009) synthesized carbonates of mixed cation content (Fe, Ca and Mg) from an aqueous solution at 298 and 343 K within less than 7 months. Low-temperature (<373 K) regimes in different geological environments provide feasible boundary conditions for the formation of 'natural magnesite–siderite solid solutions' displaying 'a significant incorporation of $CaCO_3$ (up to 20 mol%) in their structures' (Romanek *et al.* 2009). Although our approach is not adequate to retrace the dynamic processes of solid solution carbonate formation, it enables us to identify possible hydrogeochemical prerequisites for Mg–Fe–Ca carbonate formation and preservation in aqueous solutions. Such hydrogeochemical processes should trigger activities of dissolved species$_{(aq)}$ in aqueous solutions sufficient to achieve ion activity products greater than Mg–Fe–Ca carbonate solubility products.

MODELING RESULTS

Several modeling scenarios with various preassigned modeling conditions are considered. We varied: (i) the pathway of equilibration with mineral phases (re-equilibration; suppression of re-equilibration), (ii) CO_2 partial pressure (de-and increasing), (iii) water-to-rock ratios and (iv) temperature. The parameter values tested in the different scenarios are listed in Table 2. The results of nine different scenarios will be discussed. The scenario names (e.g. r-d-438-303) indicate: (i) re-equilibration or suppressed re-equilibration ('r-'or 's-'), (ii) decreasing, increasing or constant CO_2 partial pressure ('d-', 'i-' or 'c-'), (iii) water-to-rock ratio ('4380-', '438-' or '43.8-') and (iv) temperature or temperature range ('303', '278', '348' or '348/278'). Five scenarios named r-d-… consider complete re-equilibration and decreasing CO_2 partial pressure at different temperatures (303, 278 or 348 K) and varying water-to-rock ratio (438, 4380 or 43.8). Scenario r-i-438-303 considers increasing CO_2 partial pressure and complete re-equilibration at 303 K and a water-to-rock ratio of 438. Scenario s-d-438-303 considers suppressed re-equilibration (303 K; water-to-rock ratio 438) while pCO_2 is decreasing. Scenario r-d-438-348/278 considers decreasing temperature (348 to 278 K) and complete re-equilibration while pCO_2 is decreasing (water-to-rock ratio 438). The last scenario r-c-438-348/278 considers a constant pCO_2 (0.1013 MPa) coupled to decreasing temperature (348 to 278 K; complete re-equilibration; water-to-rock ratio 438).

Effect of water-to-rock ratios on equilibrium species distribution

Scenarios r-d-4380-303, r-d-438-303 and r-d-43.8-303

We calculated the equilibrium species distribution in the modeling reactors for varying water-to-rock ratios (4380, 438 and 43.8 mol mol^{-1}), decreasing pCO_2 (from 10.1325 to 0.0001 MPa) and complete re-equilibration at 303 K. The equilibration leads to: (i) complete dissolution of all primary silicate phases, (ii) negligible dissolution and precipitation of pyrite, (iii) dissolution and precipitation of hydroxyapatite, (iv) massive precipitation of ternary solid solution carbonate and $SiO_{2(a)}$ coupled to minor precipitation of Ca montmorillonite and (v) precipitation of magnetite coupled to precipitation of Mg-rich carbonate (for details, see Table S10; scenario r-d-438-303). The equilibrium conditions of the aqueous solution display free proton and corresponding electron activities ranging between pH 4.8 and pe −0.9 (pCO_2 10.1325 MPa) to pH 8.1 and pe −5.3 (pCO_2 0.0001 MPa). For a water-to-rock ratio of 438 mol mol^{-1} and pCO_2 decreasing from approximately 6 to 0.0001 MPa, the modeled compositional variation resembles the measured major element composition of FDCP in ALH84001 (for the compositional zoning trend of secondary carbonate, see Fig. 2).

A similar compositional variation occurs for simulations considering a lower water-to-rock ratio of 43.8 mol mol^{-1}

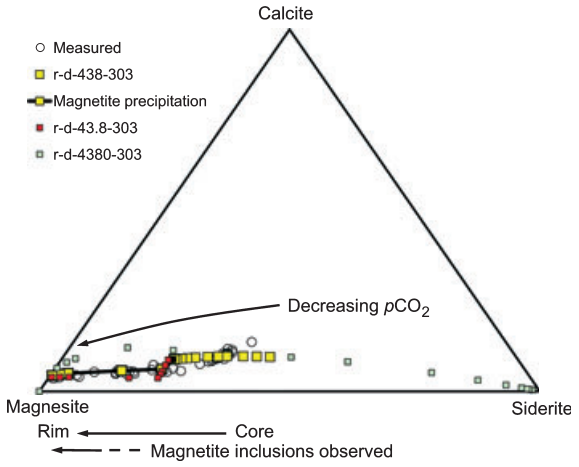

Fig. 2. Modeled compositional variation of solid solution carbonate. Modeling scenarios 1d-438-30, 1d-43.8-30, and 1d-4380-30 (1d: complete re-equilibration and decreasing pCO_2; 438 or 43.8 or 4 380: water-to-rock ratio; 30: 30°C/303K). Range of modeled compositional variation leading to magnetite precipitation is presented separately for scenario 1d-438-30. Measured major element composition of ALH84001 carbonates (see Fig. 1 for comparison).

(scenario r-d-43.8-303). However, this resulting compositional variation is limited to Mg-rich and Fe-poor carbonate. The depressed compositional variation is achieved by a larger 'CO_2 buffer capacity' which is provided by the relatively larger quantity of primary silicate minerals at a lowered water-to-rock ratio of 43.8 mol mol^{-1}. Increasing the level of pCO_2 to approximately 101 MPa from 10.1325 MPa at a water-to-rock ratio of 43.8 mol mol^{-1} is still insufficient to match observations (result not presented in Fig. 2 and Table 2).

The modeled compositional zoning expands over the measured range to a nearly pure siderite at a higher water-to-rock ratio of 4 380 mol mol^{-1} and elevated levels of pCO_2 (Fig. 2; scenario r-d-4380-303), due to a lower 'CO_2 buffer capacity'. Moreover, the modeled compositional variation at a water-to-rock ratio of 4380 mol mol^{-1} deviates from the trend of measured composition of FDCP in ALH84001 (Fig. 2).

Effect of increasing pCO_2 on equilibrium species distribution

Scenario r-i-438-303

Although the results from modeling scenario r-i-438-303 are not presented in detail here, we note that magnesite-rich carbonate is precipitated first (at low levels of increasing pCO_2) followed by the precipitation of magnesio-sideritic carbonate (at elevated levels of pCO_2). The resulting inverse compositional zoning trend reflects an inverse development of pCO_2.

Effect of increasing temperature on equilibrium species distribution

Scenarios r-d-438-278, r-d-438-303 and r-d-438-348

We also evaluated the effect of different temperatures (278, 303 and 348 K) on species distribution at equilibrium. At a water-to-rock ratio of 438 mol mol^{-1}, with pCO_2 decreasing from 10.1325 to 0.0001 Mpa, complete re-equilibration is achieved (Fig. 3: modeling scenarios, r-d-438-278, r-d-438-303 and r-d-438-348). In contrast to results at high equilibrium temperatures, modeled compositional variations at lower temperatures and decreasing pCO_2 (approximately 1 to 0.0001 Mpa at 278 K; approximately 6 to 0.0001 Mpa at 303 K) reflect the trend of measured major element composition of FDCP and the observed precipitation of magnetite coupled to precipitation of Mg-rich carbonate in ALH84001. Equilibration at 278 K (scenario r-d-438-278) results in higher siderite contents at pCO_2 higher than approximately 1 MPa. The sideritic component is limited at high temperatures (348 K), even at the highest pCO_2 (10 MPa).

Effect of decreasing temperature (decreasing or constant pCO_2) on equilibrium species distribution

Scenarios r-d-438-348/278 and r-c-438-348/278

Scenarios r-d-438-348/278 and r-c-438-348/278 were calculated to evaluate the effect of decreasing temperature (348 to 278 K) on species distribution at equilibrium. At a water-to-rock ratio of 438 mol mol^{-1}, pCO_2 decreasing from 10.1325 to 0.0001 MPa (scenario r-d-438-348/278)

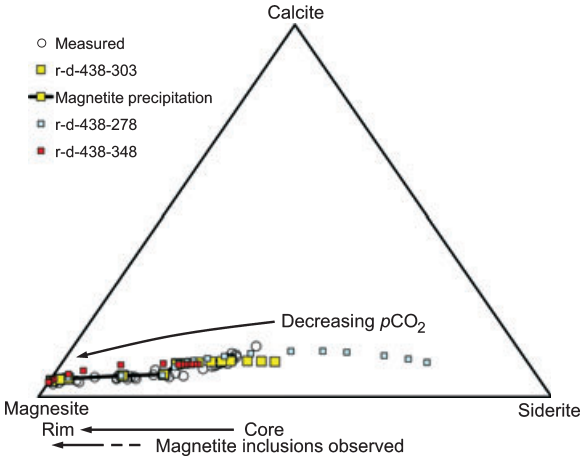

Fig. 3. Modeled compositional variation of solid solution carbonate. Modeling scenarios 1d-438-30, 1d-438-5, and 1d-438-75 (1d: complete re-equilibration and decreasing pCO_2; 438: water-to-rock ratio; 30 or 5 or 75: 30°C/ 303K or 5°C / 278K or 75°C / 348K). Range of modeled compositional variation leading to magnetite precipitation is presented separately for scenario 1d-438-30. Measured major element composition of ALH84001 carbonates (see Fig.1 for comparison).

or constant at 0.1 MPa (scenario r-c-438-348/278), entire re-equilibration is achieved while temperature is decreasing. Modeling results (Fig. 4: scenarios r-c-438-348/278 and r-d-438-348/278) indicate that decreasing temperature at constant pCO_2 leads to compositional variation of solid solution carbonate from magnesite (core; formed at 348 K) to magnesio-siderite (rim; formed at 278 K). By contrast, FDCP in ALH84001 displays the reverse trend of compositional variation [from magnesio-siderite (core) to magnesite (rim)]. Moreover, FDCP's observed broad range of compositional variation is not retraced, and the modeled compositional variation is limited to medium and low contents of sideritic component (Fig. 4). The combination of decreasing pCO_2 and decreasing temperature (scenario r-d-438-348/278; Fig. 4) yields FDCP's overall trend of compositional variation from magnesio-siderite (core) to magnesite (rim). By contrast, FDCP's observed broad range of compositional variation is not retraced, and modeled compositional variation is limited to medium and low contents of sideritic component (Fig. 4). Both scenarios (r-c-438-348/278; r-d-438-348/278) show less congruence with measured data than scenario r-d-438-303 (Fig. 2).

Effect of suppressed re-equilibration with secondary carbonate

Scenario s-d-438-303

An alternative scenario considers suppression of re-equilibration with secondary carbonate. The controlling pCO_2 is decreased from 10.1325 to 0.0001 MPa at 303 K (water-to-rock ratio 438 mol mol^{-1}). The generated secondary carbonate lacks the observed compositional variation of FDCP in ALH84001 (results not presented in detail). Moreover,

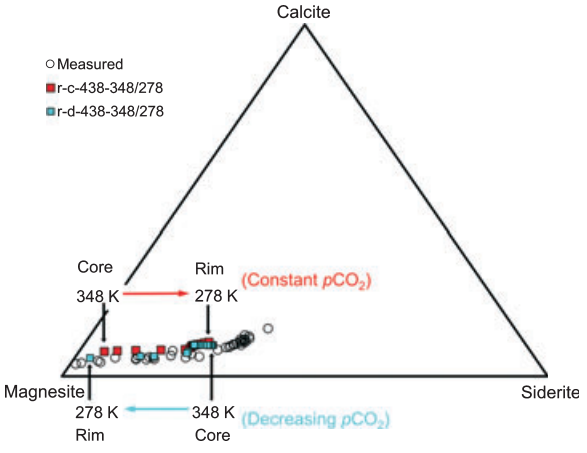

Fig. 4. Modeled compositional variation of solid solution carbonate. Modeling scenarios 3d-438-75/5 and 3c-438-75/5 (3d: decreasing pCO_2; 438: water-to-rock ratio; 75/5: decreasing temperature 75°C [348K] to 5°C [278K]; 3c: constant pCO_2; 438: water-to-rock ratio; 75/5: decreasing temperature 75°C [348K] to 5°C [278K]). Measured major element composition of ALH84001 carbonates (see Fig. 1 for comparison).

negative saturation indices prohibit precipitation of magnetite even when magnesite-rich carbonates are formed.

DISCUSSION OF RESULTS AND IMPLICATIONS

Our thermodynamically based modeling results give quantitative support to the qualitative findings that Fe- and Mg-rich aqueous solutions interacting with ultramafic rock at high pCO_2 must have a lower pH (<7) and a low temperature (<373 K) to eventually precipitate Mg–Fe–Ca carbonate similar to FDCP in a short period of time (hours or days) from a dynamic aqueous system (Niles 2005; Niles *et al.* 2006, 2009). Moreover, our modeling results indicate that: (i) the release of Mg^{2+}, $Fe^{2+}$and Ca^{2+} by dissolution of orthopyroxenite in acidified water, (ii) precipitation of $SiO_{2(am)}$, (iii) precipitation of Mg–Fe–Ca solid solution carbonate with a distinct range and compositional zoning trend, and (iv) precipitation of magnetite coupled to Mg-rich carbonate can be driven by a high and decreasing carbon dioxide partial pressure. At temperatures between 348 and 278 K, FDCP's overall compositional variation trend from magnesio-siderite (core) to magnesite (rim) is retraced by modeling scenarios which consider an isothermal temperature regime (278 or 303 K). Decreasing temperature (348 to 278 K) at constant pCO_2 results in the formation of solid solution carbonates which display a reverse compositional variation trend from magnesite (core) to magnesio-siderite (rim). This impact of decreasing temperature on the compositional variation trend is overcompensated by the effect of decreasing pCO_2 (10.1325 to 0.0001 MPa).

The compositional zoning trend of modeled solid solution carbonate is characterized by the formation of magnesio-siderite (core) at high levels of pCO_2 and to the formation of magnesite (rim) at low levels of pCO_2. Relative iron depletion and enrichment of magnesium related to a decrease in pCO_2 results from thermodynamic constraints. Thermodynamic solubility constants of solid solution carbonate end-members – siderite, magnesite and calcite – differ by more than two orders of magnitude. Siderite is characterized by a considerably lower solubility than magnesite and calcite ($FeCO_3 = Fe^{2+} + CO_3^{2-}$; $\log\_k = -10.89$; $MgCO_3 = Mg^{2+} + CO_3^{2-}$; $\log\_k = -8.029$. $CaCO_3 = Ca^{2+} + CO_3^{2-}$; $\log\_k = -8.48$; 278 K). An assumed aqueous solution at 278 K that is characterized (for the sake of simplicity) by an activity of free $Fe^{2+}_{(aq)}$ ions ($a Fe^{2+}_{(aq)}$) that equals the activity of free $Mg^{2+}_{(aq)}$ ions at a given activity of free $CO^{2-}_{3(aq)}$ ions ($a CO^{2-}_{3(aq)}$) assists in explaining why higher pCO_2 favors Fe-rich solid solution carbonates while lower pCO_2 favors Mg-rich carbonates. Assumed activity of $CO^{2-}_{3(aq)}$ is too low to achieve positive saturation indices ($SI_{siderite}$ and $SI_{magnesite}$) at given activities of $Fe^{2+}_{(aq)}$ ($=a Mg^{2+}_{(aq)}$) due to low pH at starting conditions. A stepwise increase in $a CO^{2-}_{3(aq)}$ due to increasing pH of the aqueous

solution would first lead to siderite saturation. Siderite would precipitate while magnesite's SI is still negative if only the pure end-members are considered. Therefore, siderite is characterized by a greater 'pH stability' (stable at lower pH) compared with magnesite. Higher pCO_2 leads to lower pH, and thus to the precipitation of siderite. Thermodynamic equilibrium constants of the pure end-members – siderite and magnesite (and calcite) – govern the composition and mass transfer of ternary solid solution carbonate. As ideal behavior of all components is assumed and activity coefficients for components of solid solution carbonate phases and miscibility gaps are not considered, decreasing pCO_2 will lead to the precipitation of Fe-rich carbonates first at high pCO_2 (approximately 10 MPa) and low pH if solid solution carbonate is considered. Model systems exposed to a high initial pCO_2 are characterized by the lowest pH (pH 4.8; Table S10). Ongoing precipitation of Fe-rich carbonates would drive the activity ratio $a\mathrm{Fe}^{2+}_{(aq)}/a\mathrm{Mg}^{2+}_{(aq)}$ towards more Mg-rich conditions in the aqueous solution. Moreover, lower pCO_2 (higher pH) would favor the precipitation of Mg-rich carbonates. FDCP's compositional variation varies from magnesio-siderite (Fe-rich core) to magnesite (Mg-rich rim) and is retraced by modeling scenarios which consider decreasing pCO_2. In scenarios which consider decreasing temperature, FDCP's observed that the range of compositional variation is not retraced, and modeled compositional variation is limited to medium and low contents of sideritic component. Increasing temperature (278–348 K) produces the same overall effect on the compositional variation of solid solution carbonate (decreasing the sideritic component) as decreasing pCO_2.

CONCLUSIONS

At the water-to-rock ratios, pCO_2 and temperatures considered, interactions of primary silicate phases with the aqueous solution are unlikely to reach solubility equilibrium. These interactions are predominantly irreversible. The primary silicate phases of the phase assemblage in the reactor (Table 1) can be completely dissolved in 1.0 l of the aqueous solution. The resulting negative saturation indices indicate that the applied equilibrium constants are not key factors controlling the modeled interactions of primary silicate phases with the aqueous solution. By contrast, the type and amount of primary silicate phases are key factors. Within our preferred scenarios of complete re-equilibration at 303 or 278 K, decreasing pCO_2 from approximately 1 to 0.0001 MPa at 278 K or from approximately 6 to 0.0001 MPa at 303 K, and a water-to-rock ratio of 438, equilibration leads to: (i) complete dissolution of all primary silicate phases, (ii) negligible dissolution and precipitation of pyrite, (iii) dissolution and precipitation of hydroxyapatite, (iv) massive precipitation of ternary solid solution carbonate and $SiO_{2(a)}$ coupled to minor precipitation of Ca montmorillonite and (v) precipitation of magnetite coupled to precipitation of Mg-rich carbonate. The modeled compositional variation of the solid solution carbonate resembles the measured major element composition of FDCP in ALH84001 and its compositional zoning trend.

A high and decreasing carbon dioxide partial pressure can trigger hydrogeochemical conditions enabling the formation of a secondary mineral phase assemblage with distinct composition (including Mg–Fe–Ca carbonate with a distinct trend of compositional zoning, $SiO_{2(am)}$, magnetite). Formation of a secondary phase assemblage similar to FDCP in the ALH84001 meteorite can be enabled by low-temperature and isochemical weathering reactions of orthopyroxenite in water. A key factor is a dynamic gas pressure regime with decreasing pCO_2 (approximately 1 to 0.0001 MPa at 278 K or approximately 6 to 0.0001 MPa at 303 K) during subsurface weathering.

PROBABLE SETTING ON EARLY MARTIAN SURFACE

Although our hydrogeochemical models are of a generic nature, we propose a geological setting for FDCP formation in ancient Martian crust. Environments capable of FDCP formation require: (i) orthopyroxenite-bearing rocks less than approximately 500 m below the Martian surface, (ii) adequate surface temperatures and thermal gradients, (iii) groundwater infiltration into fractures of the host rock, (iv) accumulation of CO_2 in a sealed aquifer, (v) an anoxic atmosphere with pCO_2 in the range of 0.01 to 0.0001 MPa, and (vi) cap rock disintegration to enable degassing of $CO_{2(g)}$ towards atmospheric pCO_2 conditions.

The crystallization age of orthopyroxenite in ALH84001 is estimated to be 4.5 Gyr (Nyquist *et al.* 2001) and FDCP formation 0.5–0.6 Gyr later (Corrigan & Harvey 2004). The first ALH84001 shock event is speculated to be 4.0 Gyr in age (Ash *et al.* 1996), and is argued to have fractured the orthopyroxenite (McKay *et al.* 1996). Weak greenhouse models suggest that Martian surface temperatures may have remained below freezing throughout heavy bombardment in the Late Noachian (approximately 4.0 to 3.8 Gyr). At the end of heavy bombardment, temperatures may have remained close to freezing even with strong greenhouse situations characterized by a thick H_2O–CO_2 atmosphere with elevated levels of pCO_2 (0.05–0.1 MPa; Carr 1999). The existence of groundwater reservoirs (Treiman 2008) locally sealed by an impermeable cryospheric layer is one consequence of the climatic conditions at the end of heavy bombardment. CO_2 hydrate would accumulate above CO_2-charged groundwater, with thickening cryosphere extending downwards into the stability field of CO_2 hydrate. The low thermal conductivities of gas hydrate may permit existence of liquid water in

near-surface groundwater reservoirs (Kargel *et al.* 2007). Resulting pCO_2 may reach elevated levels of 1–6.1 MPa in groundwater beneath a gas hydrate stability zone. Solubility of CO_2 in liquid and pure water inside the stability field of, and in equilibrium with, CO_2 hydrate at 278 K and 3 Mpa is in the range of 0.02 mol mol^{-1} (equivalent to approximately 1.1 mol kgw^{-1}; Zatsepina & Buffett 2001). Our modeling results (scenario r-d-438-278 indicate that siderite-rich carbonate with FDCP's core composition is precipitated at 278 K when decreasing pCO_2 achieves approximately 1 MPa. Coexisting aqueous solutions (scenario r-d-438-278) are characterized by high carbon dioxide concentrations in the range of 1.4 to 0.7 mol kgw^{-1} (pCO_2: 2 to 1 MPa) and enable coexistence of CO_2 hydrate at 278 K (pCO_2: 2 MPa). These high pCO_2 and aqueous carbon dioxide concentrations could drive precipitation of magnesio-siderite cores and amorphous SiO_2 coupled to intense dissolution of orthopyroxenite in a sealed groundwater reservoir.

Pulses of high heat flow due to increased volcanic activity or effects induced by the thermally insulating layers of CO_2 hydrate (Kargel *et al.* 2007) could have triggered the dissociation of CO_2 hydrate, fracturing of sealing cryosphere and outbursts of liquid water and $CO_{2(g/aq)}$ from the aquifer. 'Local CO_2-driven water fountains' (Bargery *et al.* 2008) may lead to a rapid decrease in pCO_2 towards atmospheric conditions and induce the precipitation of magnesite-rich rims with magnetite inclusions. Our modeling results (scenario r-d-438-278) indicate that magnesite-rich carbonate (>70 mol% $MgCO_3$; including magnetite) with FDCP's rim composition is precipitated at 278 K when decreasing pCO_2 achieves approximately 0.001 MPa. Coexisting aqueous solutions are characterized by low carbon dioxide concentrations in the range of 0.007 to 0.006 mol kgw^{-1} (pCO_2: 0.001 to 0.0005 MPa) which prevent formation of stable CO_2 hydrate and may lead to further dissociation and destabilization of sealing CO_2 hydrate. Our proposed scenario ends with subsequent shock events, which (partly) thermally decompose Fe-bearing carbonate and promote additional magnetite formation (Brearley 1998).

ACKNOWLEDGEMENTS

We thank H.-M. Schulz, E. Hauber and P.B. Niles for a valuable discussion. Our manuscript has been notably improved by the reviewer J. Palguta.

REFERENCES

Ash RD, Knott SF, Turner G (1996) A 4-Gyr shock age for a martian meteorite and implications for the cratering history of Mars. *Nature*, **380**, 57–9.

Bargery A, Wilson L, Neather A (2008) CO_2-driven water fountains during water release events on Mars. *Lunar Planetary Science*, **XXXIX**, abstr. 1102.

Bernas MP, Clemett SJ, Thomas-Keprta KL, McKay DS, Gibson EK (2005) FIB microscopy of Martian meteorite ALH84001 carbonate disks. *Microscopy and Microanalysis*, **11**, 832–3.

Brearley AJ (1998) Magnetite in ALH84001: product of the decomposition of ferroan carbonate. *Lunar Planetary Science*, **XXIX**, abstr. 1451.

Carr MH (1999) Retention of an atmosphere on early Mars. *Journal Geophysical Research*, **104**, 21897–909.

Corrigan CM, Harvey P (2004) Multi-generational carbonate assemblages in martian meteorite Allan Hills 84001: implications for nucleation, growth, and alteration. *Meteoritics & Planetary Science*, **39**, 17–30.

Dreibus G, Jagoutz E, Spettel B, Wänke H (1996) Phosphate-mobilization on Mars? Implication from leach experiments on SNC's. *Lunar Planetary Science*, **XXVII**, 323–4.

Eiler JM, Valley JW, Graham CM, Fournelle J (2002) Two populations of carbonate in ALH84001: geochemical evidence for discrimination and genesis. *Geochimica et Cosmochimica Acta*, **66**, 1285–303.

Golden DC, Ming DW, Schwandt CS, Morris RV, Yang SV, Lofgren GE (1999) An experimental study on kinetically-driven precipitation of Ca–Mg–Fe carbonates from solution: implications fort he low-temperature formation of carbonates in martian meteorite ALH84001. *Lunar Planetary Science*, **XXX**, abstr. 1973.

Golden DC, Ming DW, Schwandt CS, Lauer HV Jr, Socki RA, Morris RV, Lofgren GE, McKay GA (2001) A simple inorganic process for formation of carbonates, magnetite, and sulfides in Martian meteorite ALH84001. *American Mineralogist*, **86**, 370–5.

Greenwood JP, McSween HY (2001) Petrogenesis of Allan Hills 84001: constraints from impactmelted feldspathic and silica glasses. *Meteoritics & Planetary Science*, **36**, 43–61.

Greenwood JP, Mojzsis SJ, Coath CD (2000) Sulfur isotopic compositions of individual sulfides in Martian meteorites ALH84001 and Nakhla: implications for crust-regolith exchange on Mars. *Earth and Planetary Science Letters*, **184**, 23–5.

Harvey RP, McSween HY (1994) Ancestor's bones and palimpsests: olivine in ALH84001 and orthopyroxene in Chassigny. *Meteoritics*, **29**, 472.

Harvey RP, McSween HY (1996) A possible high-temperature origin for the carbonates in the martian meteorite ALH84001. *Nature*, **382**, 49–51.

Hurowitz JA, McLennan SM (2007) A ~3.5 Gyr record of water-limited, acidic weathering conditions on Mars. *Earth and Planetary Science Letters*, **260**, 432–43.

Kargel JS, Furfaro R, Prieto-Ballesteros O, Rodriguez JAP, Montgomery DR, Gillespie AR, Marion GM, Wood SE (2007) Martian hydrogeology sustained by thermally insulating gas and salt hydrates. *Geology*, **35**, 975–8.

Mautner MN, Sinaj S (2002) Water-extractable and exchangeable phosphate in Martian and carbonaceous chondrite meteorites and in planetary soil analogs. *Geochimica et Cosmochimica Acta*, **66**, 3161–74.

McKay DS, Gibson EK Jr, Thomas-Keprta KL, Vali H, Romanek CS, Clemett SJ, Chillier XDF, Maechling CR, Zare RN (1996) Search for past life on Mars: possible relic biogenic activity in Martian meteorite ALH84001. *Science*, **273**, 924–30.

McSween HY, Harvey RP (1998) An evaporation model for formation of carbonates in the ALH84001 Martian meteorite. *International Geology Review*, **40**, 774–83.
Meyer C (2003) Mars meteorite compendium, X1-X-22. http://curator.jsc.nasa.gov/antmet/mmc/mmc.htm.
Mittlefehldt DW (1994) ALH84001. A cumulate orthopyroxenite member of the Martian meteorite clan. *Meteoritics*, **29**, 214–21.
Niles PB (2005) Evaluation of the formation environment of the carbonates in Martian meteorite ALH84001. *Dissertation Arizona State University*.
Niles PB, Zolotov MY, Leshin LA (2006) The role of CO_2 in aqueous alteration of ultra-mafic rocks and the formation of Mg-, Fe-rich aqueous solutions on early Mars. *Lunar Planetary Science*, **XXXVII**, abstr. 1440.
Niles PB, Zolotov MY, Leshin LA (2009) Insights into the formation of Fe- and Mg-rich aqueous solutions on early Mars provided by the ALH 84001 carbonates. *Earth and Planetary Science Letters*, **268**, 122–30.
Nyquist LE, Bansal BM, Wiesmann H, Shih CY (2001) Ages and geologic histories of Martian meteorites. *Space Science Reviews*, **96**, 105–64.
Owen BB, Brinkley SR (1941) Calculation of the effect of pressure upon ionic equilibria in pure water and in salt solutions. *Chemical Reviews*, **29**, 461–74.
Parkhurst DL, Appelo CAJ (1999) User's guide to PHREEQC (version 2) – a computer program for speciation, batch-reaction, one-dimensional transport, and inverse geochemical calculations. US Geological Survey Water-Resources Investigations Report 99-4259.
Renard F, Gundersen E, Hellmann R, Collombet M, Le Guen Y (2005) Numerical modeling of the effect of carbon dioxide sequestration on the rate of pressure solution creep in limestone: preliminary results. *Oil & Gas Science and Technology – Rev. IFP*, **60**, 381–99.
Romanek CS, Grady MM, Wright IP, Mittlefehldt DW, Socki RA, Pillinger CT, Gibson EK (1994) Record of fluid–rock interactions on Mars from the meteorite ALH84001. *Nature*, **372**, 655–7.
Romanek CS, Jiménez-López C, Navarro AR, Sánchez-Román M, Sahai N, Coleman M (2009) Inorganic synthesis of Fe-Ca-Mg carbonates at low temperature. *Geochimica et Cosmochimica Acta*, **73**, 5361–76.
Scott ERD (1999) Origin of carbonate-magnetite-sulfide assemblages in Martian meteorite ALH84001. *Journal of Geophysical Research*, **104**, 3803–13.
Scott ERD, Krot AN, Yamaguchi A (1998) Formation of preimpact, interstitial carbonates in the Allan Hills 84001 Martian meteorite. *Meteoritic & Planetary Science*, **33**, A139–40.
Thomas-Keprta KL, Romanek C, Wentworth SJ, McKay DS, Fisler D, Golden DC, Gibson EK (1997) TEM analysis of fine-grained minerals in the carbonate globules of Martian meteorite ALH84001. *Lunar Planetary Science*, **XXVIII**, 1433–4, abstr. 1461.
Treiman AH (1995) A petrographic history of martian meteorite ALH84001: two shocks and an ancient age. *Meteoritics*, **30**, 294–302.
Treiman AH (2008) Ancient groundwater flow in the Valles Marineris on Mars inferred from fault trace ridges. *Nature Geoscience*, **1**, 181–3.
Treiman AH, Romanek CS (1998) Bulk and stable isotopic compositions of carbonate minerals in Martian meteorite Allan Hills 84001: no proof of high formation temperature. *Meteoritic & Planetary Science*, **33**, 737–42.
Valley JW, Eiler JM, Graham CM, Gibson E, Romanek C, Stolper EM (1997) Low temperature carbonate concretions in the martian meteorite ALH84001: evidence from stable isotopes and mineralogy. *Science*, **275**, 1633–8.
Warren PH (1998) Petrologic evidence for low-temperature, possibly flood evaporitic origin of carbonates in the ALH84001 meteorite. *Journal of Geophysical Research*, **103**, 16759–73.
Westall F, Gobbi P, Gerneke D, Mazzotti G (1998) Microstructures in the carbonate globules of Martian meteorite ALH84001: preliminary results of a high resolution SEM study. *Lunar Planetary Science*, **XXIX**, abstr. 1362.
Zatsepina OY, Buffett BA (2001) Experimental study of the stability of CO_2-hydrate in a porous medium. *Fluid Phase Equilibria*, **192**, 85–102.

SUPPORTING INFORMATION

Additional Supporting Information may be found in the online version of this article:

Tables S1–S9 are provided to run PHREEQC modeling with original input files and input files modified by readers. Fig. S1 is provided as an Excel file to encourage plotting of modeled results from selected output files. The link to US Geological Survey's *PHREEQC Welcome Page* is given to enable a free download of PHREEQCWin.

Table S1. Phreeqc input file for scenario r-d-438-303.

Table S2. Phreeqc input file for scenario r-d-4380-303.

Table S3. Phreeqc input file for scenario r-d-43.8-303.

Table S4. Phreeqc input file for scenario r-d-438-278.

Table S5. Phreeqc input file for scenario r-d-438-348.

Table S6. Phreeqc input file for scenario r-i-438-303.

Table S7. Phreeqc input file for scenario s-d-438-303.

Table S8. Phreeqc input file for scenario r-d-438-348/278.

Table S9. Phreeqc input file for scenario r-c-438-348/278.

Table S10. Selected output file (in parts) for scenario r-d-438-303.

Figure S1. Excel file to encourage plotting of modeled results from selected output files.

Please note: Wiley-Blackwell are not responsible for the content or functionality of any supporting materials supplied by the authors. Any queries (other than missing material) should be directed to the corresponding author for the article.